A First Order Phase Transition Underlies the Formation of Sub-Diffractive Protein Aggregates in Mammalian Cells

Arjun Narayanan[1], Anatoli B. Meriin[2], Michael Y. Sherman[2], Ibrahim I. Cissé[1]

1. Department of Physics, MIT, Cambridge, MA
2. Department of Biochemistry, Boston University School of Medicine, Boston, MA

Correspondence: Ibrahim Cissé, icisse@mit.edu

ABSTRACT: Failure in protein quality control can often lead to protein aggregation, yet in neuro-degenerative diseases, by the time aggregates can be seen, the cells have advanced well into the disease pathology. Here, we develop a quantitative imaging approach to study the protein aggregation process in living mammalian cells with unprecedented spatio-temporal resolution. We find that sub-diffractive precursor aggregates may form even in untreated cells, and their size distribution is exactly as predicted for a system undergoing a first order phase transition. Practically, this implies that as soon as aggregates reach a critical size (Rc $= 162 \pm 4$ nm in untreated cells), they will spontaneously grow into large inclusions. Our data suggest that a previously uncharacterized, RuvBL1 dependent mechanism clears aggregates above the critical size. Our study unveils the existence of sub-diffractive aggregates in living cells; and the strong agreement between cellular data and a nucleation theory, based on first order phase transition, provides insight into regulatory steps in the early stages of aggregate formation in vivo.

Neurodegenerative diseases, such as Parkinson's Disease, Amyotrophic Lateral Sclerosis, and Alzheimer's Disease, are characterized by the appearance of large protein aggregates in cells and in the extracellular space (*1*). It is hypothesized that intermediate species in the aggregation process are likely more toxic moieties (*2-9*) than conventionally visible large aggregates, plaques or fibres. However detecting and characterizing intermediate aggregates remains a fantastic technical challenge. Capturing the early steps of protein aggregation in living cells can help uncover hidden mechanisms in their formation and regulation in vivo, as well as elucidate their putative roles in protein misfolding diseases (*2-9*).

Here we develop a quantitative super-resolution assay to study the early steps protein aggregation in mammalian cells. We adopt proteasome inhibition as an approach used to study the formation of large aggregates in living mammalian cells (*10-12*). Treatment of cells with the proteasome inhibitor MG132 (*13*) leads to the gradual accumulation of misfolded, aggregation-prone proteins, and to the formation of the aggresome, a large juxta-nuclear inclusion body akin to Lewy bodies (*14, 15*) in Parkinson's disease cells. We engineered mammalian cell lines expressing Synphilin 1 - a marker of aggregates in Parkinson's disease (*10, 16, 17*) - fused to a fluorescent protein Dendra2 (*18*). Dendra2 is a green to red photo-convertible protein that enables photo-activation localization microscopy (PALM) (*19*), a single-molecule based super-resolution (*19-21*) approach we used previously to quantitatively image protein clustering with high spatio-temporal resolutions in living cells (*22, 23*).

Imaging Synphilin 1 by conventional fluorescence, shows emergence of the aggresome around 135 minutes after treatment (**Fig. 1A-E**, top panels and **supplementary movie 1)** but formation dynamics of the aggresome cannot be readily measured with this imaging approach. Instead, when we perform live cell super-resolution imaging (*24*) (**Fig. 1A-E**, bottom panels), we can detect and quantify the growth of individual aggresomes (**Fig. 1F**), from their inception at length scales unattainable in previous live cell studies (*25*). Furthermore, in addition to the large aggresome, the examination of **Fig. 1A-E** (bottom panels and **supplementary movie 1**) shows a population of sub-diffractive aggregates throughout the cellular cytoplasm and indiscernible in the conventional

images (top panels). Thus, our live cell super-resolution imaging approach reveals a previously undetected population of sub-diffractive aggregates.

We characterize the properties of these sub-diffractive aggregates using density based spatial clustering of applications with noise (DBSCAN) (*26*). We record for each aggregate, the radius, and the number of localization events (fluorescence detection events) ((*24*) and **supplementary text 1**). Only aggregates with a radius greater than our localization accuracy (estimated to be ~20nm (*22*)) are interpreted in our analysis; aggregates of radius less than 25nm are discarded.

As represented in **Fig. 1G,** we find that the number of localization events per aggregate is proportional to the radius cubed (volume) of the aggregate (also **supplementary text 1**). This observation implies that sub-diffractive aggregates have a defined density, with the aggregate size scaling linearly with volume. Relying on the precise number of molecular detections to estimate aggregate size can be complicated by single molecule photo-physical variability (*27*). Here, we rely on the existence of a well-defined density to use the spatial extent (radius cubed) of the aggregate as the measure of the size. For subsequent theoretical analyses, we found it practical to define the aggregate size as a reduced numerical parameter '*n*' (see **supplementary text 1**, and **Fig. S1**].

Previous studies, from experiments done in vitro, have invoked nucleation and growth as a potential mechanism underlying aggregate formation (*28*). However, such models imply that aggregation occurs through a first order phase transition into a so-called state of *super-saturation*, characterized by a well-defined nucleation barrier (*29*). The nucleation barrier reflects a critical aggregate size above which spontaneous growth is energetically favoured, and below which aggregate disassembly is favoured. Such a critical aggregate size, if it exists, has been difficult to measure experimentally (*28*), due in part to the challenge of detecting the stochastically formed, transient precursor clusters; and it is unclear even if proven in vitro, whether phase transition formalism may still hold inside the cells where complex biological quality control mechanisms exist. If a first order phase transition is pertinent, there are clear theoretical expectations for the distribution and evolution of aggregate sizes. Therefore, we investigate the mechanism behind sub-diffractive aggregates

formation and growth in mammalian cells, initially, by studying the size distribution of the aggregates, and how the distribution evolves with time.

In nucleation and growth a system may be either in a *sub-saturated* state (**Fig. 2A**), or in a *super-saturated* state (**Fig. 2B** & **C**). In the first case the formation and growth of sub-diffractive aggregates is not favoured energetically. In such a *sub-saturated* system, an exponential distribution of aggregate sizes is expected (*29, 30*). For a *sub-saturated* state, the overall distribution of aggregate sizes does not change with time even as individual aggregates may grow or disassemble (**supplementary text 2**, and simulations in **Fig. 2D**).

Alternatively, in a *super-saturated* state, the system is poised such that aggregates that stochastically reach the critical size become energetically favoured to grow spontaneously (see **supplementary text 2** and **Fig. S2**). In such a case the distribution of aggregate sizes is time-evolving (simulations in **Fig. 2E**& **F**) and may result in a peak at large aggregate sizes when the total pool of contributing proteins is conserved (**Fig. 2E**). Alternatively , the pool of contributing proteins may be continuously replenished, leading to an exponential distribution of small aggregates coexisting with a growing shoulder at larger aggregate sizes (**Fig. 2F**); This may likely be the case in living cells when new misfolded proteins can constantly be added to the system. As represent in **Fig. 2G** our super-resolution data reveals a distribution of aggregate sizes with a shoulder growing towards larger aggregates, as a function of time after treatment, more consistent with the simulations in **Fig. 2F**. This result suggests that sub-diffractive aggregate formation and time evolution may behave as a *super-saturated* condensation system.

A *super-saturated* system is expected to exhibit precise energetics, underlain by a critical aggregate size (*29*) (noted here as n_c or R_c). n_c is the point at which the surface energy cost is balanced by the minimising energy of the molecules buried in the bulk of the aggregate. In particular the expected form of the free energy cost to form a aggregate of size "n", is given by $U(n) = an^{2/3} - bn$, with two terms ($an^{2/3}$ and bn) representing the surface and bulk contributions respectively (**supplementary text 2**, and **Fig. S2**). Moreover, in this formalism, for aggregates below the critical

size (i.e $n < n_c$) the Boltzmann distribution ($P(n) \propto e^{-U(n)}$), the equilibrium thermodynamics exponentially-suppressed distribution, would be expected even though the full system may not be in equilibrium (*29*).

We examine whether the sub-diffractive aggregates in the mammalian cells truly exhibit such stringent energetics. Given that for a *super-saturated* system the sub-critical aggregate ($n < n_c$) size distribution may be approximated as $P(n) \propto e^{-U(n)}, n < n_c$, , then the negative logarithm should give the free energy cost $U(n)$, i.e $-Log\big(P(n)\big) \propto U(n)$, for $n < n_c$. By plotting the negative logarithm of the size distribution one can test how well the distribution is governed by the precise free energy cost $U(n) = an^{2/3} - bn$ (see prediction in **Fig. 3A**). We find a remarkable agreement between the experimentally measured sub-critical size distribution shown in **Fig. 3B** and this very specific prediction of simple condensation theory (see (*24*) and **supplementary text 2**).

The agreement between theory and experiment in **Fig. 3B** involves a fit with two model-parameters (surface and bulk terms respectively). We test even further whether the two terms can be decoupled. That is, whether a fit of the only the surface term at a physically appropriate limit, would result in a data-set which is accounted for primarily by the remaining bulk term.

The surface term ($an^{2/3}$) must dominate for very low-n. Thus we posit that by fitting only the first few data points of the $-Log\big(P(n)\big)$ graph to the surface term $an^{2/3}$, and subtracting it off of the data (*24*), then for all remaining sub-critical aggregates the resultant should be the volume term, i.e. $\left[-Log\big(P(n)\big) - an^{\frac{2}{3}}\right] \propto -bn$. This resultant should be a straight line when plotted versus aggregate size n, (see theoretical prediction in **Fig. 3C**). We note that there is, a-priori, nothing else in our dataset imposing that the resulting data should be linear upon correction of the surface term. Thus if the data deviate from the first order phase transition energetics, we would expect a scattered resultant, or the revelation of a different energy dependence. In **Fig. 3D** the data show a strikingly linear resultant, demonstrating a high quality agreement between the theory and super-resolution experimental data.

From the results in **Fig. 3**, therefore, we conclude that while other bio-regulatory processes might be at play, the simple condensation picture with specific energetic dependence $U(n) = an^{2/3} - bn$, describes how sub-diffractive aggregates can form and grow to a well-defined critical size n_c in the mammalian cells. We also tested aggregates with the Neuro2A cell line (neuronal precursor cells, see **supplementary text 3**) and observe the very same conclusions (**Fig. S3**) suggesting the physical mechanism for sub-diffractive aggregation may be general to a range of mammalian cells.

Biochemically, the specific parameters in the energetics for nucleation and growth would depend on the concentration of aggregating proteins and on their effective energy of interactions. To further test this notion, we sought to increase the concentration of misfolded aggregating polypeptides in living cells by incubation with a proline analog azetidine-2-carboxylic acid (AZC). This molecule incorporates in newly synthesized polypeptides instead of proline, and prevents normal folding, thus generating a massive build-up of misfolded proteins in the cell (*31*). In a condensation model, such a build-up would result in a greater degree of *super-saturation* with a stronger bulk (linear) term.

We find in **Fig. 3E&F** that the distribution of aggregates sizes in the presence of AZC fits the same functional form, and with a larger linear slope indicative of a larger bulk term (also see further AZC characterization in **supplementary text 4**, **Fig. S4** and general applicability of our results under other perturbations in **supplementary text 5**, **Fig. S5**). The AZC incubation data further validates the agreement between cellular aggregation data and the nucleation model, and with interpretations consistent with that expected of a classical *super-saturated* system.

Implicit to phase transition theory is the notion that any cell including healthy cells or those untreated with proteasome inhibitor, may readily form sub-diffractive aggregates which spontaneously grow into large inclusions after reaching n_c. This expectation is counter to a widely held belief that the presence of precursor aggregates may directly indicate cell pathology (*2*). In **Fig. 4A** (left panel) we find that untreated cells do in fact show sub-diffractive aggregates implying that aggregates readily formed inside the cell without chemical treatments.

However, untreated cells are distinctly void of large super-critical aggregates. A violin plot of aggregate sizes from untreated cells (**Fig. 4C**, black) indicates that while a large population of small aggregate sizes is apparent (indicated by the width of the violin plot in **Fig. 4C**), untreated cells do not have a significant population of large aggregates. For instance we rarely found aggregates of radius greater than 250nm in untreated cells. We measure the critical radius to be R_c =162±4 nm for untreated cell (**Fig. 4D**, black bar, see Supplementary text 2 for calculation of n_c or R_c). Therefore, despite the fact that clusters should reach n_c and then stably grow, such a population of super-critical clusters seems to be suppressed in healthy cells. These results imply that a hidden mechanism may exist to clear the cells of super-critical aggregates (i.e. aggregates that have reached sizes greater that the critical radius) in untreated cells.

We sought to test whether a clearance pathway could account for the absence of super-critical aggregates in untreated cells. Because a AAA+ ATPase, RuvBL, was previously suggested as a potential protein disaggregase in mammalian cells and in yeast (*32*), we tested whether RuvBL may be involved in the preferential clearance of super-critical aggregates. We find that knocking down RuvBL1 in untreated cells, results in the appearance of large aggregates (**Fig. 4B**, compare to untreated cell **Fig. 4A**). A violin plot of aggregate sizes from RuvBL1 knocked-down cells shows a clear population of large aggregate sizes, with some aggregates with radii greater than $1\mu m$, a size range that could only be observed previously after hours of proteasome inhibition (**Fig. 4C**). These results implicate RuvBL1 in the clearance of large aggregates from untreated cells (see **supplementary text 6**, and **Fig. S6** for further tests of RuvBL1).

Importantly, we find that upon RuvBL1 knockdown, $R_c = 157 \pm 6\, nm$ did not change significantly from R_c in control untreated cells ($162 \pm 4\, nm$) (**Fig. 4D**) suggesting that RuvBL1 knockdown did not significantly change the sub-critical distribution. This observation implies that RuvbL1 did not affect the concentration of aggregating molecules or their interactions, unlike, for instance, proteasome inhibition which gradually reduced R_c (**Fig. 4D**). Indeed, depletion of RuvBL1 prevented clearance of large aggregates following washout of MG132 without affecting either the distribution of aggregates in the sub-critical range or R_c (**supplementary text 6** and **Fig. S6**). Our data

indicate that RuvBL1 dependent clearance of aggregates acts specifically on aggregates that have reached a size above R_c, without changing the nucleation process.

The measured critical sizes, R_c, range from ~160 nm in untreated or siRNA knockdown cells, to ~120 nm 3 hours after proteasome inhibition. These small magnitudes for R_c indicate that a super-resolution technique is needed to unveil and measure this transition point *in vivo*, as by the time individual aggregates are sufficiently large to be detected in conventional cell imaging techniques they are already in the post-nucleation regime.

Previous studies bypass the direct observation of a nuclear barrier, and observe instead a sigmoidal response in the number of visible aggregates (*28*). This signmodial response is characterized by a lag-time followed by rapid growth after nucleation when a sufficiently large number of aggregates have crossed the nucleation barrier. However in the living cell, biological mechanisms may intervene in the post-nucleation regime to regulate the presence of larger aggregates.

Our results indicate that a hidden pathway may exist to clear cells of aggregates above the critical size, and we have identified RuvBL1 as a necessary effector in this putative super-critical clearance pathway. The mechanism by which RuvBL1, and perhaps other effectors work to preferentially clear super-critical aggregates in the cell remains currently unknown. Nonetheless, the agreement between our cellular super-resolution data and condensation systems with first order phase transition opens an avenue in the study of protein aggregation, whereby detailed theoretical predictions may be proposed and falsified experimentally, directly with quantitative *in vivo* imaging.

While our investigation has focused on aggregates related to Parkinsons disease, we note that the methodology can be readily extended to any protein that can be fluorescently tagged (for example fused to the GFP-like Dendra2). Thus we anticipate that this approach can help address protein aggregation in a broad range of cellular processes or disease pathologies.

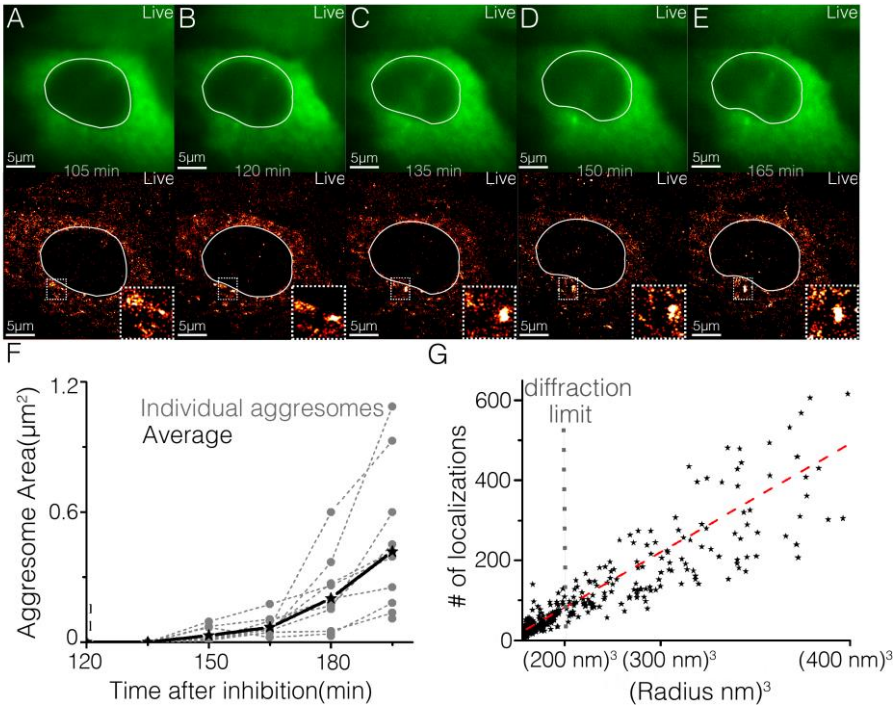

Figure 1: ***Super-resolution imaging of Synphilin1-Dendra2 in live mammalian cells recapitulates aggresome formation and shows the existence of sub-diffractive aggregates.***

A-E Conventional imaging of Pre-converted Dendra2 (GFP-like) signal (top panels) and Super-resolution localization map of Photo-converted Dendra2 signals(bottom panels) in a living cell expressing Synphilin1-Dendra at time points: between 105 to 165 minutes of incubation with proteasome inhibitor MG132. Both conventional and super-resolved imaging show the formation of an aggresome and development of a kidney shaped nucleus, but in addition the super-resolved images show both more detailed and earlier visible aggresome as well as a large population of sub-diffractive aggregates. Insets: detailed view of the evolving aggresome. **F** Growth of aggresomes in ten cells. **G** Super-resolution microscopy approach allows quantitative assessment of aggregate sizes besides the aggresome. We find the number of localizations – proportional to the number of molecules in the aggregate – scales as the cube of the radial spread up to the apparent focal depth of our 2-dimensional microscope (see **supplementary text 1** for details). Therefore (a) radius cubed reflects the number of molecules in the aggregate, and (b) aggregates exhibit a constant density. Data in G includes ~ 4000 found aggregates from 6 cells incubated with MG132 for 120 minutes

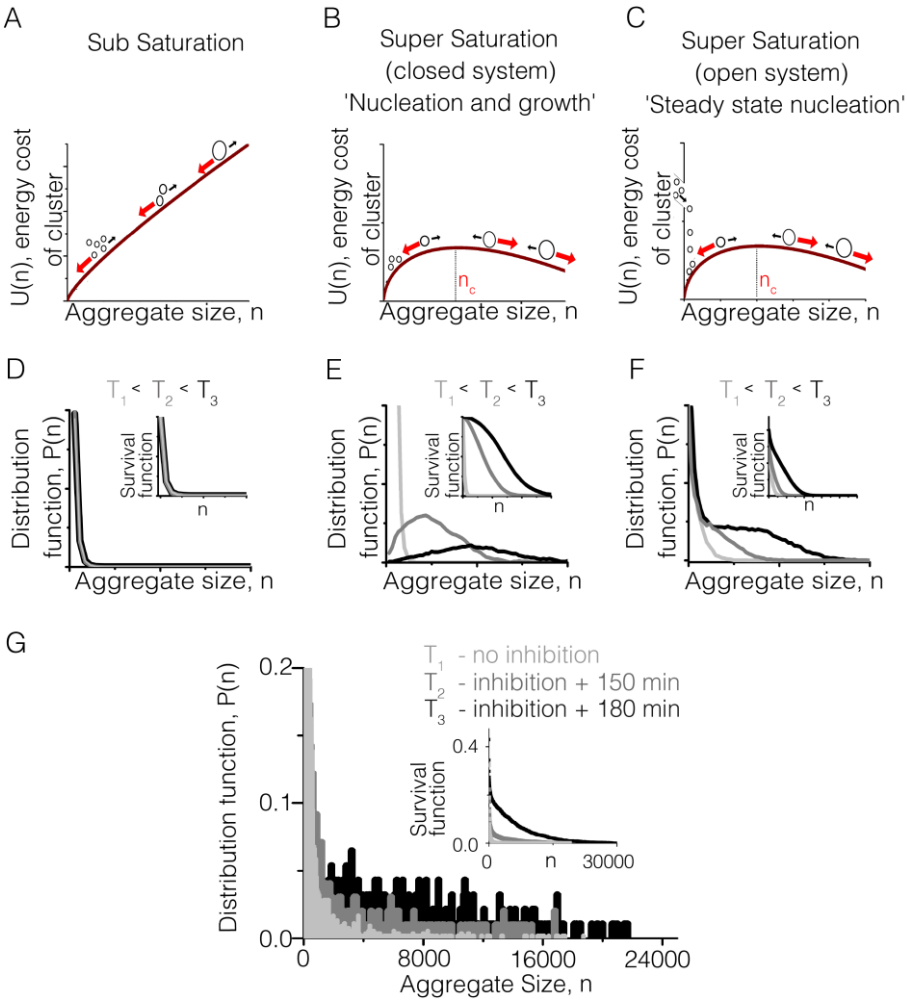

Figure 2: Similarities between the experimental data on evolution of Synphillin1 aggregates upon proteasome inhibition and expectations from systems in condensing systems: A-C Size dependent free energy cost of aggregate formation for various scenarios - **A** A *sub-saturated* system where the vapor phase is the thermodynamically favored ground state (**supplementary text 2**). **B** A closed *super-saturated* system. where the system evolves to the aggregated (condensed) phase. **C** An open *super-saturated* system with constant monomer replenishment. Similar to B but with constant creation of new vapor even as the system evolves towards the aggregated (condensed) state. **D** Time independent, exponential size distribution (simulated) and resulting survival function (inset) in the *sub-saturated* phase. **E** Time evolving size distribution (simulated) and resulting survival function (inset) in the *super-saturated* case as the system evolves to one large aggregate of system size. **F** Time evolving shoulder of large aggregates coexisting with a continuously replenished population of small aggregates and resulting survival function (inset) in the case of a *super-saturated* system with constant monomer input (simulated). **G** Experimentally determined aggregate size distributions in untreated cells (light grey), cells after 150 minutes of proteasome inhibition (grey) and cells after 180 minutes of proteasome inhibition (dark grey) - resulting survival function in inset. Note the similarity to sub-figure **F**. Data in **G** represents the normalized distributions from 10000 aggregates (light grey) from 10 untreated cells, 6500 aggregates (grey) from 8 cells and 4000 (dark grey) from 10 cells**.** Details of simulation in **D-F** in (*24*)

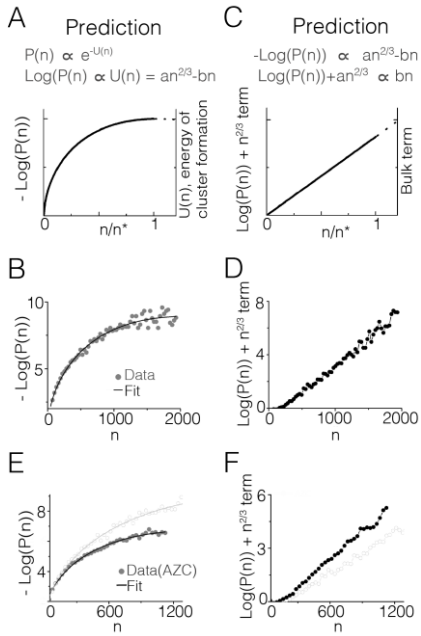

Figure 3: Aggregate size distributions are well described by condensation theory. A The expected sub-critical aggregate size distribution in the case of a *super-saturated* vapor is $P(n) \propto e^{-U(n)}; With\ U(n) = an^{2/3} - bn.$ [**supplementary text 2**]. $an^{2/3}$ is a measure of surface tension of the condensing aggregates while $-bn$ is a measure of the bulk energy gain from n molecules joining an aggregate. Plotting $-Log\big(P(n)\big)$ therefore directly gives us access to the energy function U(n). **B** The measured sub-critical aggregate size distribution from untreated cells and its fit to the form $-Log\big(P(n)\big) \propto bn + an^{2/3}$ **C** The expected sign of the *b* in the energy cost function for the *super-saturated* case is positive and this can be extracted from the experimentally measured $Log\big(P(n)\big)$ by fitting the low n values to a pure $n^{2/3}$ dependence and subtracting away this dependence to leave the purely linear bulk term (bn) **D** The $-bn$ term in the energy cost function extracted from the data is both strikingly linear and its positive slope implies untreated cells are *super-saturated*. **E** The measured sub-critical aggregate size distribution from azetidine-2-carboxylic acid treated cells and its fit to the form $-Log\big(P(n)\big) \propto bn + an^{2/3}$(grey circles and black line) with light grey circles and line for comparison to untreated cells. **F** The $-bn$ term in the free energy cost function extracted from the data in the case of azetidine-2-carboxylic acid treated cells (black circles) remains linear and its positive slope is increased compared to data from untreated cells (light grey circles) consistent with an *super-saturation*. Untreated cell data is from the normalized distribution of 10,000 aggregates from 10 cells and AZC data from 4000 aggregates from 7 cells

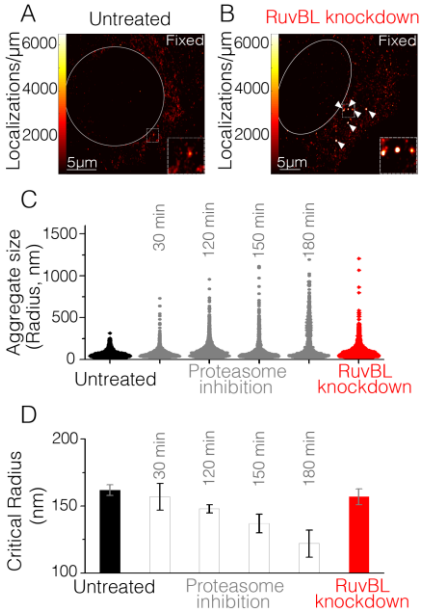

Figure 4: RuvBL1 dependent mechanism may clear super-critical aggregate in untreated cells. **A** Representative super-resolved localization heat map for an untreated cell showing many sub-diffractive aggregates but few large aggregates (white line delineates nucleus). **B** Representative super-resolution localization maps with RuvBL1 depletion showing the cytoplasmic accumulation of super-critical aggregates marked by white arrows (white line delineates nucleus). Insets in **A, B** show detailed view of the largest aggregates in each condition. **C** Violin plots showing the distribution of observed aggregate radii in the untreated (black), proteasome inhibited (grey) and RuvBL1 depleted (red) cases. Untreated cell data is from the normalized distribution of 10,000 aggregates from 10 cells, RuvBL1 knockdown of 8000 aggregates from 9 cells, and inhibition data of 5000-8000 aggregates from 6-10 cells per time point. **D** The effect of proteasome inhibition (grey bars) and RuvBL1 depletion (red bar) on the critical radius, which in unperturbed cells (black bar) is ~ 162 nm. Unlike proteasome inhibition the effect of RuvBL1 depletion on the condensation energetics and consequently on the critical radius is small [error bars represent errors in fit estimation as explained in(*24*)].

References:

1. D. J. Selkoe, Cell biology of protein misfolding: the examples of Alzheimer's and Parkinson's diseases. *Nat Cell Biol* **6**, 1054-1061 (2004).
2. C. A. Ross, M. A. Poirier, Protein aggregation and neurodegenerative disease. *Nat Med* **10 Suppl**, S10-17 (2004).
3. M. R. Cookson, The biochemistry of Parkinson's disease. *Annu Rev Biochem* **74**, 29-52 (2005).
4. J. Xu *et al.*, Dopamine-dependent neurotoxicity of alpha-synuclein: a mechanism for selective neurodegeneration in Parkinson disease. *Nat Med* **8**, 600-606 (2002).
5. N. Gosavi, H. J. Lee, J. S. Lee, S. Patel, S. J. Lee, Golgi fragmentation occurs in the cells with prefibrillar alpha-synuclein aggregates and precedes the formation of fibrillar inclusion. *J Biol Chem* **277**, 48984-48992 (2002).
6. D. L. Pountney *et al.*, Annular alpha-synuclein species from purified multiple system atrophy inclusions. *J Neurochem* **90**, 502-512 (2004).
7. D. P. Karpinar *et al.*, Pre-fibrillar alpha-synuclein variants with impaired beta-structure increase neurotoxicity in Parkinson's disease models. *EMBO J* **28**, 3256-3268 (2009).
8. H. A. Lashuel *et al.*, Alpha-synuclein, especially the Parkinson's disease-associated mutants, forms pore-like annular and tubular protofibrils. *J Mol Biol* **322**, 1089-1102 (2002).
9. H. A. Lashuel, D. Hartley, B. M. Petre, T. Walz, P. T. Lansbury, Neurodegenerative disease: amyloid pores from pathogenic mutations. *Nature* **418**, 291 (2002).
10. M. Tanaka *et al.*, Aggresomes formed by alpha-synuclein and synphilin-1 are cytoprotective. *J Biol Chem* **279**, 4625-4631 (2004).
11. N. Zaarur, A. B. Meriin, V. L. Gabai, M. Y. Sherman, Triggering aggresome formation. Dissecting aggresome-targeting and aggregation signals in synphilin 1. *J Biol Chem* **283**, 27575-27584 (2008).
12. J. A. Johnston, C. L. Ward, R. R. Kopito, Aggresomes: a cellular response to misfolded proteins. *J Cell Biol* **143**, 1883-1898 (1998).
13. A. F. Kisselev, A. L. Goldberg, Proteasome inhibitors: from research tools to drug candidates. *Chem Biol* **8**, 739-758 (2001).
14. K. S. McNaught, P. Shashidharan, D. P. Perl, P. Jenner, C. W. Olanow, Aggresome-related biogenesis of Lewy bodies. *Eur J Neurosci* **16**, 2136-2148 (2002).
15. C. W. Olanow, D. P. Perl, G. N. DeMartino, K. S. McNaught, Lewy-body formation is an aggresome-related process: a hypothesis. *Lancet Neurol* **3**, 496-503 (2004).
16. K. Wakabayashi *et al.*, Synphilin-1 is present in Lewy bodies in Parkinson's disease. *Ann Neurol* **47**, 521-523 (2000).
17. K. K. Chung *et al.*, Parkin ubiquitinates the alpha-synuclein-interacting protein, synphilin-1: implications for Lewy-body formation in Parkinson disease. *Nat Med* **7**, 1144-1150 (2001).
18. D. M. Chudakov, S. Lukyanov, K. A. Lukyanov, Tracking intracellular protein movements using photoswitchable fluorescent proteins PS-CFP2 and Dendra2. *Nat Protoc* **2**, 2024-2032 (2007).
19. E. Betzig *et al.*, Imaging intracellular fluorescent proteins at nanometer resolution. *Science* **313**, 1642-1645 (2006).
20. M. J. Rust, M. Bates, X. Zhuang, Sub-diffraction-limit imaging by stochastic optical reconstruction microscopy (STORM). *Nat Methods* **3**, 793-795 (2006).
21. S. T. Hess, T. P. Girirajan, M. D. Mason, Ultra-high resolution imaging by fluorescence photoactivation localization microscopy. *Biophys J* **91**, 4258-4272 (2006).
22. W. K. Cho *et al.*, RNA Polymerase II cluster dynamics predict mRNA output in living cells. *Elife* **5**, (2016).
23. I. I. Cisse *et al.*, Real-time dynamics of RNA polymerase II clustering in live human cells. *Science* **341**, 664-667 (2013).
24. Materials and methods are available as supplementary materials.

25. F. Opazo, A. Krenz, S. Heermann, J. B. Schulz, B. H. Falkenburger, Accumulation and clearance of alpha-synuclein aggregates demonstrated by time-lapse imaging. *J Neurochem* **106**, 529-540 (2008).
26. M. Ester *et al.* (AAAI Press, Proceedings of the Second International Conference on Knowledge Discovery and Data Mining (KDD-96), 1996), pp. 226-231.
27. S. H. Lee, J. Y. Shin, A. Lee, C. Bustamante, Counting single photoactivatable fluorescent molecules by photoactivated localization microscopy (PALM). *Proc Natl Acad Sci U S A* **109**, 17436-17441 (2012).
28. A. M. Morris, M. A. Watzky, R. G. Finke, Protein aggregation kinetics, mechanism, and curve-fitting: a review of the literature. *Biochim Biophys Acta* **1794**, 375-397 (2009).
29. V. V. Slezov, *Kinetics of first order phase transitions*. (Wiley-VCH, Weinheim, 2009), pp. xiv, 415 p.
30. F. F. Abraham, *Homogeneous nucleation theory; the pretransition theory of vapor condensation*. Advances in theoretical chemistry Supplement (Academic Press, New York,, 1974), pp. xiv, 263 p.
31. A. L. Goldberg, A. C. St John, Intracellular protein degradation in mammalian and bacterial cells: Part 2. *Annu Rev Biochem* **45**, 747-803 (1976).
32. N. Zaarur *et al.*, RuvbL1 and RuvbL2 enhance aggresome formation and disaggregate amyloid fibrils. *EMBO J* **34**, 2363-2382 (2015).

Statement of Conflict of interests: The authors declare no conflict of interests

Acknowledgments: We thank Kabir Ramola (Brandeis), Jeff Gore (MIT), Kandice Tanner (NCI/NIH) as well as members of the Cissé lab at MIT (Jan Hendrik Spille, and Micca Hecht) for helpful comments and discussions. Research reported in this publication was supported by the National Cancer Institute and the National Institutes of Health through the NIH Director's New Innovator Award Number DP2CA195769 to IIC. The content is solely the responsibility of the authors and does not necessarily represent the official views of the National Institutes of Health. This work was also supported by funds from the MIT Department of Physics.

Supplementary Materials:

Materials and Methods

Supplementary text 1-6

Tables S1-S6

Movies S1